Desalination and Water Treatment
www.deswater.com

doi: 10.5004/dwt.2017.20903

78 (2017) 49–56
June

Evaluation of a mixture of amines for the preparation of the polyamide layer of the thin-film nanocomposite membranes for forward osmosis

Rajesha Kumar*, Maha Salman, Saleh Al-Haddad

Water Research Center, Kuwait Institute for Scientific Research, P.O. Box 24885, 13109 Safat, Kuwait, Tel. +965 97920482; emails: ralambi@kisr.edu.kw (R. Kumar), matallah@kisr.edu.kw (M. Salman), shaddad@kisr.edu.kw (S. Al-Haddad)

Received 9 November 2016; Accepted 10 May 2017

ABSTRACT

Thin-film nanocomposite (TFN) forward osmosis membranes were prepared by incorporating halloysite nanotubes (HNTs) into the polyamide layer which formed by the interfacial polymerization (IP) reaction between the mixture of amines polyethylenimine (PEI): *m*-phenylenediamine (1:1) and trimesoyl chloride on the surface of polysulfone substrate. The surface hydrophilicity of the membranes was evaluated using contact angle goniometer. The surface morphological features of membranes were determined using atomic force microscope and field emission scanning electron microscope. The combined effect of using 1:1 mixture of amines with increased loading of HNTs into polyamide layer altered the membrane morphology first from nodular structures to ridge valley structures. Due to the presence of PEI during the IP process the resultant membranes experienced increased smoothness for the loading of HNTs. The loading of 0.05 wt% of HNT termed as an optimized composition and this membrane witnessed maximum flux of 44.6 L/m^{2}h at the active layer facing draw solution mode with relatively less reverse solute flux of 4.2 gMH. The TFN membranes exhibited stable flux during the fouling tests and easy cleaning efficiency due to their smooth and hydrophilic surfaces.

Keywords: Thin-film nanocomposite membrane; Polyethyleneimine; *m*-phenylenediamine; Antifouling

1. Introduction

Thin-film composite (TFC) membranes are widely used in reverse osmosis and nanofiltration. In recent years, another potential application of TFC membranes in forward osmosis (FO) process was extensively explored. The major benefit of TFC membrane over conventional cellulose triacetate membranes is their flexibility in design as both the selective and support layers can be tailored for specific needs [1,2]. A TFC membrane comprised of an aromatic polyamide thin film formed by the interfacial polymerization (IP) process on top of an asymmetric polymer membrane support layer. The substrate layer of the TFC membrane decides flux and it should be porous with low structural parameter to minimize the internal concentration polarization (ICP) [1]. The structural properties of polyamide (PA) layer will be greatly affected by the nature of monomers used during the IP reaction [3,4]. The other parameters such as the concentration of monomers, reaction time and temperature will alter the performance of TFC membrane. Recently, the incorporation of small quantities of nanomaterial into PA layer has shown much improvement in FO performance of the membranes [2,5–7]. The resultant membranes are generally called as thin-film nanocomposite (TFN) membranes.

Halloysite nanotube (HNT) nanoclay is potential fillers for polymeric membranes due to their large surface area, high length-to-diameter (L/D) ratio and good physicochemical properties [8]. HNTs are natural occurring clay particles much cheaper than other nanosized materials [9]. It consists of a 1:1 aluminosilicate layer with abundant Si–OH and Al–OH groups, which provide strong hydrophilic nature to HNTs. In addition, HNTs offer the benefits such as good stability, high rejection against organic solvents and ease of disposal or reusability that are needed for membrane making [10]. However, incorporation of neat HNTs into active PA layer is a difficult task due to their agglomeration effect [11].

* Corresponding author.

Generally, a PA layer will be formed by IP reaction between acyl chloride and an amine. *m*-Phenylenediamine (MPD) and trimesoyl chloride (TMC) are most commonly used monomers for IP reaction [12]. The nanomaterial can be incorporated into PA layer either by dispersing in aqueous (amine) phase or in organic (acyl chloride) phase. The selection of medium for the dispersion of nanomaterial is based on their low agglomeration effect. The aqueous MPD is the most frequently used phase for the dispersion of nanomaterial due to their high affinity toward polar water groups. However, most of the researchers experienced increased surface roughness for the TFN FO membranes with the increased loading of nanomaterial in PA layer via MPD solution [13–16]. The increased roughness has an adverse effect on the antifouling characteristics of the resultant membranes.

The different novel monomers have been explored to improve the TFC membrane performance. Among them, the replacing of the low molecular weight amines by polymeric polyethylenimine (PEI) tend to have more hydrophilic surfaces, attain positive charge on the surface, show smoother surfaces and high antifouling properties [17,18]. The lower reactivity of PEI helps to manipulate the morphological features and thickness of the resultant membrane surface by altering the temperature and reaction time during the IP process [19,20]. The macromolecular PEI having high amine group density provides a large number of reactive sites which favors the IP process [21]. Most importantly, the aqueous PEI solution has tendency to reduce the agglomeration effect among the nanomaterial and to improve their dispersion propensity [22,23].

In current work, the mixture of MPD and PEI amines were used for the coating of PA layer over polysulfone (PSF) substrate using TMC as the other monomer for the IP reaction. Further, the neat HNTs in various concentrations were incorporated into PA layer of the membranes by dispersing in the aqueous mixture of amines. The changes in morphological features of the TFN membranes by replacing of MPD solution by the equal amount of PEI solution were evaluated. Further, the combined effect of PEI and HNTs on the hydrophilicity, FO flux and antifouling characteristics of the TFN membranes were studied.

2. Experimental

2.1. Materials

PSF (molecular weight = 35,000 Da), polyethyleneimine (50% in water), HNTs and polyethylene glycol (molecular weight = 600) were purchased from Sigma-Aldrich Co. (USA) MPD and TMC were purchased from Alfa-Aesar Co. (UK) *N*-Methylpyrrolidone, *N*,*N*-dimethylformamide, sodium chloride, gypsum ($CaSO_4$. $2H_2O$) and ethanol were purchased from Merck Co. (Germany). For all FO performance experiments deionized (DI) water was used.

2.2. Preparation of TFC and TFN membranes

2.2.1. Preparation of PSF substrate layer

A two-step procedure was employed for the fabrication of both TFC and TFN membranes. In the first step, the substrate layer was fabricated by dissolving PSF (14.0 wt%) in a mixture of solvents DMF:NMP (63.0:21.0 wt%) at 60°C over 4 h using PEG (2.0 wt%) as a pore former additive. The homogeneous solution was degassed at 40°C for 4 h to remove the trapped air bubbles. The dope solution was poured onto a glass plate and cast by using a casting knife adjusted to the thickness of 150 μm. The glass plate was immediately immersed into a coagulation bath containing DI water containing 3.0 wt% of DMF at 25°C–26°C. After 20 min of the coagulation process, the coagulation bath was replaced with fresh DI water, and the membrane was allowed to stand for 24 h.

2.2.2. Preparation of polyamide layer

The top active PA layer was prepared by IP on the surface of a PSF substrate layer. The desired amount of HNTs (Table 1) was dispersed in the aqueous mixture of MPD (1.0%, w/v) and PEI (1.0%, w/v) at 1:1 ratio and sonicated for 30 min at 25°C–26°C followed by stirring for 30 min at the same temperature. The aqueous mixture of amines with HNTs was poured onto the top surface of the PSF substrate which was held horizontally for 1 min to ensure the penetration of amine solution into the pores of the substrate. The excess amine solution was then drained off from the substrate surface, and a rubber roller was used to remove the residual droplets of amine solution. Now, 0.1% (w/v) of TMC solution in *n*-hexane was poured onto the substrate surface. The excess TMC solution was drained off from the surface after 30 s and then the membrane was placed in an oven for curing at 50°C for 20 min to favor the IP reaction between PEI–TMC and MPD–TMC. Finally, the resulting membrane was rinsed with *n*-hexane solution to remove traces of unreacted TMC and washed with DI water before further characterization. A control TFC membrane (M0) was prepared with a similar procedure, but without adding any HNTs into the amine mixture using the compositions presented in Table 1.

2.3. Membrane characterization

The transmission electron microscope (TEM) images of the modified HNT were recorded using LVEM5 instrument (Delong America). The surface morphology of the membranes was recorded using Keysight 8500 field emission scanning electron microscope (FESEM), and the imaging was conducted with backscattering electrons mode to overcome charging effect. The surface contact angles of the membranes were recorded using optical contact angle and interface tension meter from USA KINO, model-SL200KB. The surface roughness parameters of the membranes were recorded using atomic force microscope (AFM) instrument from Concept

Table 1
The polyamide layer compositions of the membranes

Membrane	MPD (wt%)	PEI (wt%)	MPD:PEI	TMC (wt%)	HNT (wt%)
M0	1.0	1.0	50:50	0.2	0
M1	1.0	1.0	50:50	0.2	0.01
M2	1.0	1.0	50:50	0.2	0.05
M3	1.0	1.0	50:50	0.2	0.1

Scientific Instrument (Nano-Observer model), France, by scanning the membrane surface over 5 × 5 μm dimensions.

2.4. Determination of FO performance

FO experiments were conducted using a laboratory scale fabricated FO setup. It comprised of polytetrafluoroethylene cross-flow FO cell with outer dimensions of 12.7 × 10 × 8.3 cm (Sterlitech, USA), two pumps to maintain feed and DS flow (KNF, USA) and two flow meters (Blue-White Industries, California, USA). The cross-flow velocity of DS and FS were fixed at 0.8 L/min, and the temperature was maintained at 25°C ± 0.5°C. The membrane flux was determined in two different orientations of the membranes: active layer facing the feed solution (FS) mode and active layer facing the draw solution (DS) mode. The aqueous solutions of NaCl with 2 M and 10 mM concentrations were used as DS and FS, respectively. The water flux of the FO process, J (L/m^{2}h), was calculated from the volume changes of the FS and DS using Eq. (1):

$$J = \frac{\Delta V}{A\Delta t} \tag{1}$$

where ΔV (L) is the volume change over a predetermined time Δt (h) and A is the effective membrane surface area (m^2).

The reverse solute flux (RSF) is a measure of leakage of NaCl to the FS during the FO process. To measure the RSF value, the concentration of back diffused ions was measured in terms of conductivity using a calibrated conductivity meter (ORION STAR A-221 model, Thermo Scientific). The RSF, J_s (gMH), was determined based on the increased solute concentration (NaCl) in the feed side measured based on the conductivity measurements using Eq. (2):

$$J_s = \frac{\Delta C_t V_t}{A\Delta t} \tag{2}$$

where C_t (g/L) and V_t (L) are the reverse solute concentration and the volume of the FS, respectively, at an arbitrary time t; ΔC_t is the difference in salt concentrations of the FS at the beginning and at the end and ΔV_t is the difference in volume of the FS at the beginning and at the end of measuring test, respectively.

2.5. Fouling study of FO membranes

The fouling study was performed using sodium alginate (as a model organic foulant) and gypsum (as a model inorganic foulant) as a mixture of foulants. For both fouling and baseline experiments 4 M solution of NaCl was used as the DS. The FS for baseline experiment consists of a 10 mM solution of NaCl with zero concentrations of both alginate and gypsum. For the fouling study, the FS was replaced with a mixture of 10 mM NaCl, 200 mM alginate and 35 mM gypsum. The protocol to perform the FO membrane fouling test and cleaning experiments as follows. First, a fresh membrane sample was placed in the membrane cell in FO mode and a whole membrane system was stabilized with DI water on both sides of the membrane at 25°C ± 1°C for 30 min. The baseline experiment was performed to obtain the initial membrane flux (J_{w1}) and the normalized water flux was calculated based on the water flux decline. The fouling experiment was started at a cross-flow rate of 0.8 L/min, and at a temperature of 25°C ± 1°C. The corresponding changes in the weight of the DS were recorded, and later converted into changes in membrane flux. After the fouling trial, both sides of the membrane sample were replaced with fresh DI water. The cleaning experiment was carried out at higher cross-flow rate of 1.2 L/min over 30 min. After membrane cleaning, baseline experiment was started again to determine the membrane flux (J_{w2}), and the flux recovery ratio (FRR) was calculated using Eq. (3):

$$\mathrm{FRR}(\%) = \frac{J_{w2}}{J_{w1}} \times 100 \tag{3}$$

3. Results and discussion

3.1. Hydrophilicity of membranes

Generally, the lower contact angle of the membrane indicates the higher hydrophilicity, since it has a reverse correlation with hydrophilicity. Fig. 1 indicates the surface contact angle values of the membranes and the control TFC membrane showed highest contact angle of 56°. As shown, the water contact angle values of the TFN membranes gradually decrease with the increased loading of HNTs in the PA layer, indicating that the incorporated HNTs containing more –OH groups could enhance the hydrophilicity of the membrane significantly, and contribute to a greater water flux.

3.2. Morphology of membranes

3.2.1. TEM and FESEM analysis

The TEM analysis of HNT sample is presented in Fig. 1, and it revealed that the average diameter of the HNT was in the range of 30–80 nm and the length of HNT varied in the range of 50–380 nm with an average length of 110 nm. Hence, the HNT sample selected for the study was suitable for PA layer fabrication. The surface FESEM images of the membranes are presented in Fig. 2. The replacing of MPD solution with 50% PEI solution during the IP process resulted in more nodular structures on the membrane surface (Fig. 3(a)).

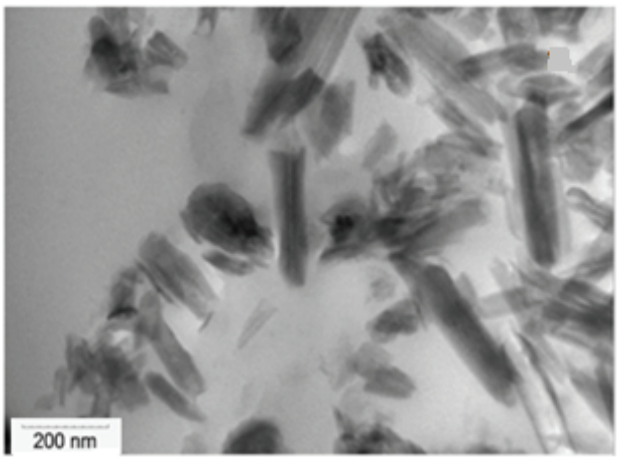

Fig. 1. The TEM image of HNT.

Generally, using 100% MPD solution will favor the formation of a ridge-valley structures on the TFC membrane surfaces as observed by the previous researchers [14–16,24]. Hence, it is worth stating that the membrane morphology changed from ridge-valley structure to nodular structure by introducing PEI during the IP process. The incorporation of HNTs resulted in the further transformation of the membrane morphological features. For the loading of 0.01 wt% of HNTs, ridge-valley structures were formed on the TFN membrane surface along with nodular structures (Fig. 3(b)). This is due to the combined effect of HNTs and PEI present during the IP process. With the increased loading of HNTs, the nodular structures reduced and more ridge-valley structures were formed on the membrane surfaces (Fig. 3(c)). This is due to the increased reaction rate between MPD–TMC and PEI–TMC during the IP process by loading HNTs [15,16]. From Fig. 3(d), the loading of 0.1 wt% of HNTs resulted in the irregular distribution of HNTs on the membrane surface due to the agglomeration effect of HNTs at excess concentration. Thus, the loading of about 0.05% HNT corresponds to the optimized loading of HNTs into the PA layer.

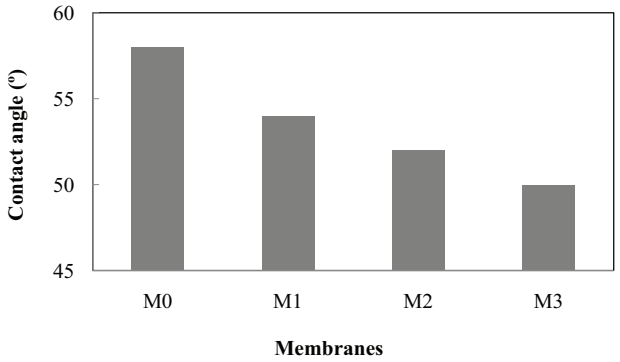

Fig. 2. The contact angle values of membranes.

3.2.2. AFM analysis

Fig. 3 represents the AFM images of TFC and TFN membranes and all the membranes exhibited relatively smooth membrane surfaces. The average roughness (R_a) values of TFN membrane surfaces decreased compared with the

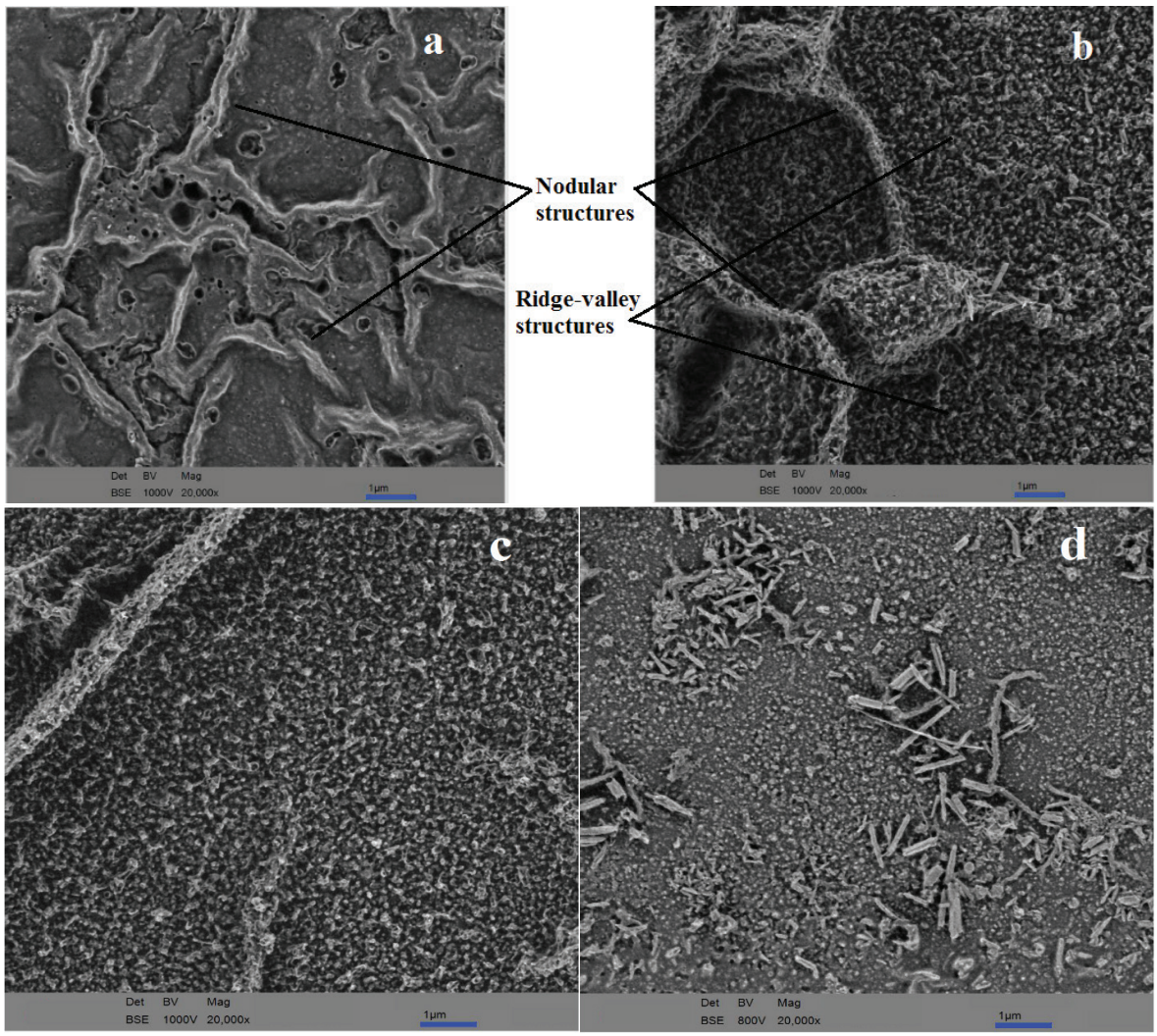

Fig. 3. FESEM images of (a) M0, (b) M1, (c) M2 and (d) M3 membranes.

control TFC membrane (M0) as a result of HNTs loading. This is attributed to the additional contribution from HNTs toward the improved IP process between both MPD–TMC and PEI–TMC [15,25]. The slow reactivity between PEI and TMC might increase in the presence of HNTs and by curing the membranes at 50°C. This might result in the formation of more PEI–TMC cross-linked amide structures on the membrane surface. The formation of such PEI–TMC cross-linked structures favored the formation of smooth membrane surfaces [3]. Further, the average roughness values of the membranes are comparable with the contact angle values of the membrane. M3 membrane loaded with highest HNTs exhibited smooth membrane surface and witnessed least contact angle value. Overall, the smooth membrane surfaces formed by the loading of HNTs resulted in reduced contact angle values and contributed to the improved hydrophilicity.

3.3. Flux and reverse solute flux of membranes

The flux of the membranes was determined at both FO and PRO modes and presented in Fig. 4. The HNTs incorporated membranes (M1–M3) showed higher flux than control M0 membrane at both orientations of the membranes. The replacing of MPD solution with 50% of PEI solution might improve the dispersion of HNTs in the selective layer. Thus, the loading of hydrophilic HNTs created additional nanopathways for the passage of water molecules [15,25–27]. Also, the excess $–NH_2$ groups of PEI macromolecules have a high tendency to wet the membrane surface and to favor the flux. However, a higher HNT concentration at 0.1 wt% lead to a less improvement in flux compared with 0.05 wt% loading. This might be due to the blockage of the water pathways by the excess HNTs due to the agglomeration effect as evidenced from Fig. 2(d).

The leakage of salt back into FS has negative impact on the overall FO performance of the membrane [28]. From Fig. 5, all the membranes consisting of PEI in the PA layer exhibited relatively lower RSF values. The M2 membrane consisting of 0.05 wt% of HNTs witnessed least RSF value with relatively high flux at both modes of operation. The same membrane displayed more ridge-valley structures on its surface as evidenced from FESEM study. The lowest RSF value for M2 membrane might be due to more cross-linked structures formed in the PA layer assisted by 0.05 wt% of

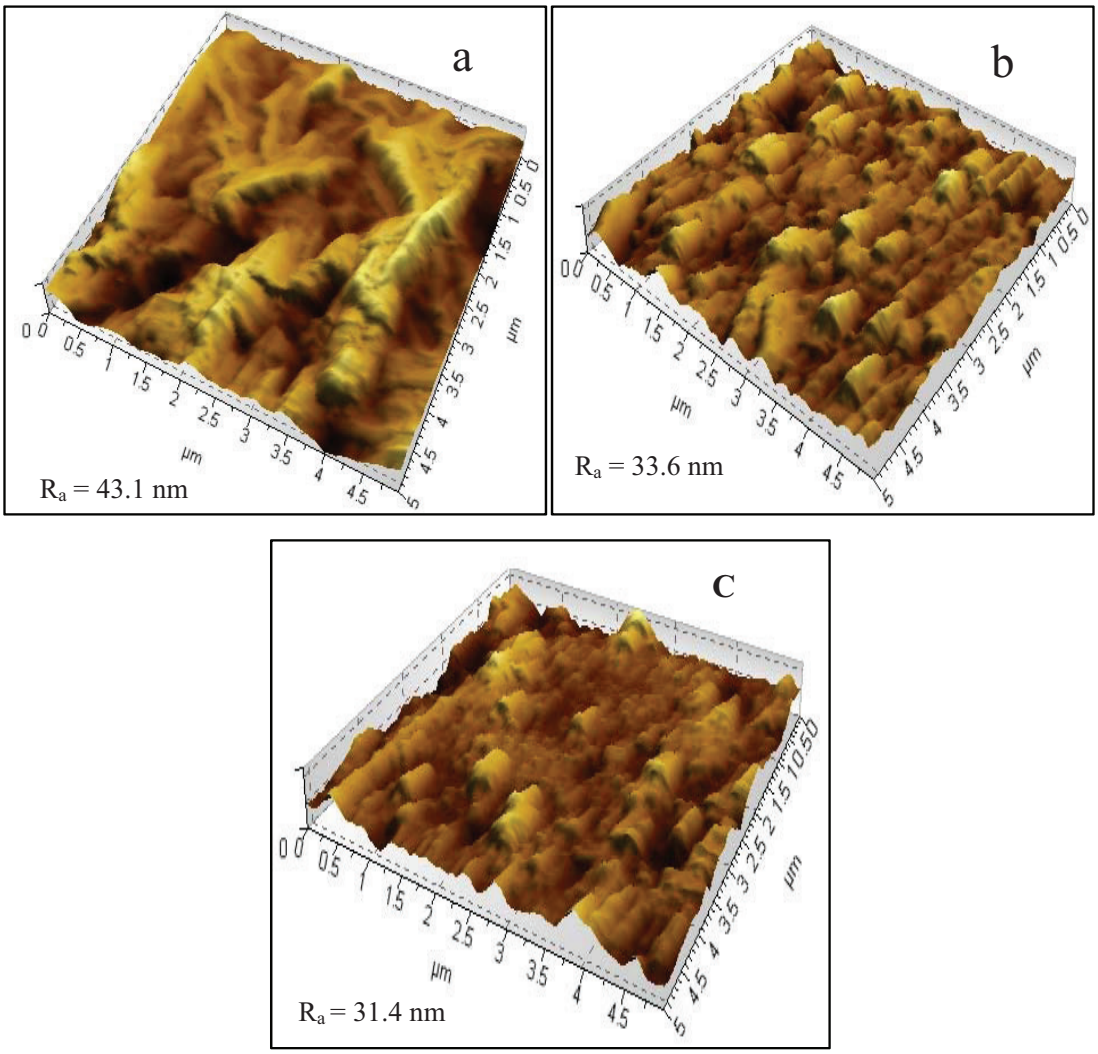

Fig. 4. AFM 3D images of (a) M0, (b) M2 and (c) M3 membranes.

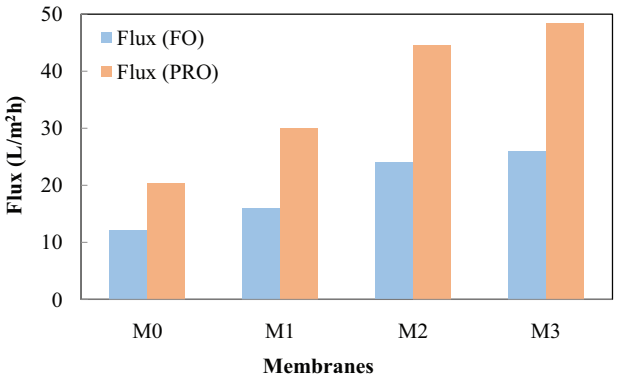

Fig. 5. Flux of the membranes at FO and PRO modes (test conditions – feed solution: 10 mM NaCl, draw solution: 2 M NaCl solution, cross-flow rate: 0.8 L/min and temperature: 25°C).

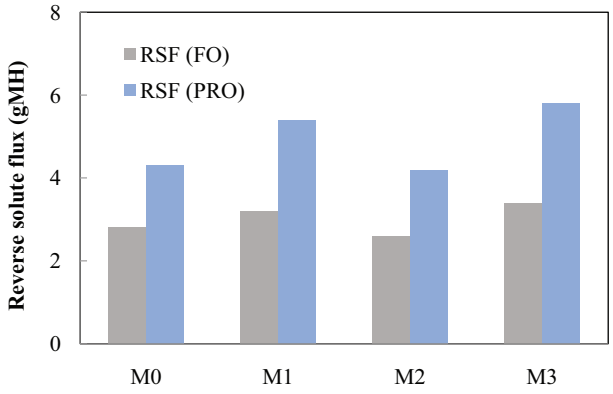

Fig. 6. The reverse salt flux of the membranes at FO and PRO modes (test conditions – feed solution: 10 mM NaCl, draw solution: 2 M NaCl solution, cross-flow rate: 0.8 L/min and temperature: 25°C).

HNTs promoting resistance to the reverse salt leakage [29]. Hence, the incorporation of HNTs up to optimized composition favored the formation of membrane structures suitable for high performance FO membranes.

3.4. Antifouling properties of the membranes

The flux change vs. time for the TFC and TFN membranes during the baseline and fouling test is presented in Fig. 6. Generally, a lower fouling curve compared with the baseline always indicates severe fouling of the membrane [30]. The observed initial flux declines for all the membranes during the fouling test due to the severe ICP offered by the membrane surface in the FO mode [31–33]. From Fig. 6, all the membranes have superior flux stability during the baseline study corresponding to the zero foulant concentration. The replacing of FS with a foulant solution from DI water resulted in the more flux reduction in the control M0 membrane corresponding to its least flux stability. However, M1–M3 TFN membranes observed much higher flux stability during the fouling test over control TFC (M0) membrane. This is due to the smooth membrane surface formed in the former with more hydrophilic surfaces. The less fouling propensity of TFN membranes also due to the combined effect of –OH groups of HNTs and excess –NH_2 groups of PEI present on the surfaces favoring the easy formation of the hydration layer at the membrane surface.

FRR is generally employed to assess the cleaning efficiency of the membranes. From Fig. 7, the M1–M4 membranes exhibited higher FRR values over the control TFC membrane signified their easy cleaning efficiencies after fouling. An interaction force among the membrane surface and the foulant are one of the critical factors governing membrane fouling phenomena [34]. The abundant –OH and –NH_2 groups present on the TFN membrane surfaces resulted in easy wetting of the membranes. Thus, the TFN membrane surfaces favored the weak binding of Ca^{2+} bridged alginate molecules present in the foulant solution. Though the foulant solution had a high concentration of gypsum the membranes experienced less scaling on the membrane surfaces. This is due to most of the Ca^{2+} ions were involved in bridging with the –COOH groups of the alginate present in the foulant solution [35]. Also, it is important to point out that the

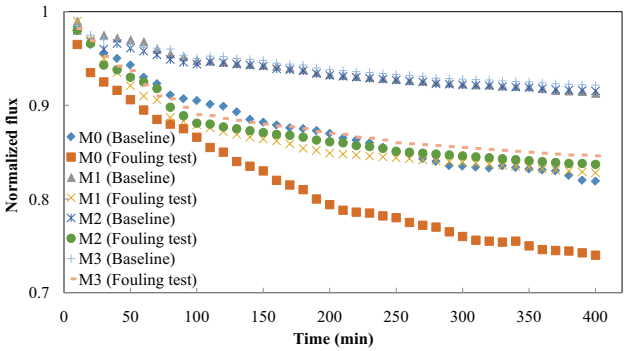

Fig. 7. The change of flux with time for the control TFC and TFN (test conditions for the baseline experiments; 4 M NaCl draw solution and 10 mM NaCl feed solution, for fouling tests; 4 M NaCl draw solution and feed solution with mixture of 10 mM NaCl, 200 mM sodium alginate and 35 mM gypsum concentrations; the normalized flux ratio was taken with a 10-min interval during the tests).

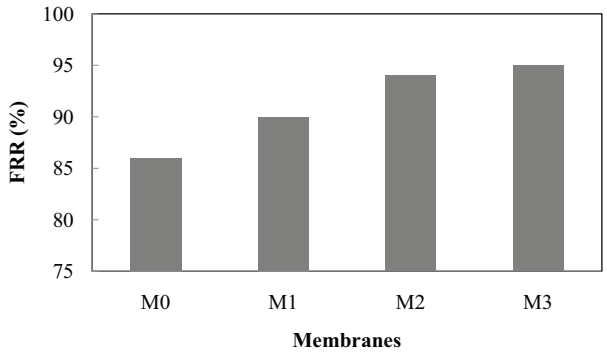

Fig. 8. The FRR values of the membranes.

hydration layer present on the membrane surface resisted the binding of Ca^{2+} ions.

4. Conclusions

TFN membranes were prepared by incorporation of different concentrations of HNTs into the PA layer formed

by interaction between mixture of amines (PEI:MPD) and TMC on PSF substrate. The contact angle study revealed the more hydrophilic nature of TFN membranes compared with control TFC membrane due to additional contribution from HNTs toward hydrophilicity. For the higher loading of HNTs, membrane surface changed from nodular structure to more ridge-valley structures. In the presence of PEI, the HNT–TFN membrane surfaces attained reduced roughness and also contributed to increased hydrophilicity. The loading of 0.05 wt% HNTs was the optimized composition for the loading of HNTs without any aggregation on the membrane surface. This composition corresponds to the high flux FO membrane with relatively less RSF. The TFN membranes exhibited good flux stability during the fouling tests conducted using a mixture of organic and inorganic foulants. The FRR of membranes increased with increased loading of HNTs attributed to their easy cleaning efficiency as presented in Fig. 8. Our study demonstrated the potentiality of using a mixture of amines toward the preparation of efficient TFN membranes for FO application.

Acknowledgments

We would like to express our gratitude to the Kuwait Institute for Scientific Research (KISR) for supporting the implementation of this research work. Furthermore, we would like to acknowledge, with much appreciation, the role of the staff of the Doha Research Station of KISR, who helped us to assembling the experimental setup and gave fruitful comments and advices.

References

[1] X. Li, K.Y. Wang, B. Helmer, T.-S. Chungnd, Thin-film composite membranes and formation mechanism of thin-film layers on hydrophilic cellulose acetate propionate substrates for forward osmosis processes, Ind. Eng. Chem. Res., 51 (2012) 10039–10050.

[2] A. Tiraferri, Y. Kang, E.P. Giannelis, M. Elimelech, Superhydrophilic thin-film composite forward osmosis membranes for organic fouling control: fouling behavior and antifouling mechanisms, Environ. Sci. Technol., 46 (2012) 11135–11144.

[3] D. Wu, Y. Huang, S. Yu, D. Lawless, X. Feng, Thin film composite nanofiltration membranes assembled layer-by-layer via interfacial polymerization from polyethylenimine and trimesoyl chloride, J. Membr. Sci., 472 (2014) 141–153.

[4] P.G. Ingole, M.I. Baig, W.K. Choia, H.K. Lee, Synthesis and characterization of polyamide/polyester thin-film nanocomposite membranes achieved by functionalized TiO_2 nanoparticles for water vapor separation, J. Mater. Chem. A, 4 (2016) 5592–5604.

[5] A. Tiraferri, Y. Kang, E.P. Giannelis, M. Elimelech, Highly hydrophilic thin-film composite forward osmosis membranes functionalized with surface tailored nanoparticles, ACS Appl. Mater. Interfaces, 4 (2012) 5044–5053.

[6] D. Emadzadeh, W.J. Lau, A.F. Ismail, Synthesis of thin film nanocomposite forward osmosis membrane with enhancement in water flux without sacrificing salt rejection, Desalination, 330 (2013) 90–99.

[7] L. Shen, S. Xiong, Y. Wang, Graphene oxide incorporated thin-film composite membranes for forward osmosis applications, Chem. Eng. Sci., 143 (2016) 194–205.

[8] H. Jing, Y. Higaki, W. Ma, J. Xi, H. Jinnai, H. Otsuka, A. Takahara, Preparation and characterization of polycarbonate nanocomposites based on surface-modified halloysite nanotubes, Polym. J., 46 (2014) 307–312.

[9] E. Abdullayev, Y. Lvov, Clay nanotubes for corrosion inhibitor encapsulation: release control with end stoppers, J. Mater. Chem., 20 (2010) 6681–6687.

[10] M. Ghanbari, D. Emadzadeh, W. Lau, T. Matsuura, A.F. Ismail, Synthesis and characterization of novel thin film nanocomposite reverse osmosis membranes with improved organic fouling properties for water desalination, RSC Adv., 5 (2015) 21268–21276.

[11] R.S. Hebbar, A.M. Isloor, K. Ananda, A.F. Ismail, Fabrication of polydopamine functionalized halloysite nanotube/polyetherimide membranes for heavy metal removal, J. Mater. Chem. A, 4 (2016) 764–774.

[12] D. Wu, Y. Huang, S. Yu, D. Lawless, X. Feng, Thin film composite nanofiltration membranes assembled layer-by-layer via interfacial polymerization from polyethylenimine and trimesoyl chloride, J. Membr. Sci., 472 (2014) 141–153.

[13] D. Emadzadeh, W.J. Lau, A.F. Ismail, Synthesis of thin film nanocomposite forward osmosis membrane with enhancement in water flux without sacrificing salt rejection, Desalination, 330 (2013) 90–99.

[14] N. Niksefat, M. Jahanshahi, A. Rahimpour, The effect of SiO_2 nanoparticles on morphology and performance of thin film composite membranes for forward osmosis application, Desalination, 343 (2014) 140–146.

[15] M. Ghanbari, D. Emadzadeh, W.J. Lau, T. Matsuura, M. Davoody, A.F. Ismail, Super hydrophilic TiO_2/HNT nanocomposites as a new approach for fabrication of high performance thin film nanocomposite membranes for FO application, Desalination, 371 (2015) 104–114.

[16] M. Amini, M. Jahanshahi, A. Rahimpour, Synthesis of novel thin film nanocomposite (TFN) forward osmosis membranes using functionalized multi-walled carbon nanotubes, J. Membr. Sci., 435 (2013) 233–241.

[17] J. Xu, Z. Wang, J. Wang, S. Wang, Positively charged aromatic polyamide reverse osmosis membrane with high anti-fouling property prepared by polyethylenimine grafting, Desalination, 365 (2015) 398–406.

[18] J.E. Cadotte, R.S. King, R.J. Majerle, R.J. Petersen, Interfacial synthesis in the preparation of reverse osmosis membranes, J. Macromol. Sci., Pure Appl. Chem., 15 (1981) 727–755.

[19] S.P. Sun, T.A. Hatton, T.S. Chung, Hyperbranched polyethyleneimine induced cross-linking of polyamide-imide nanofiltration hollow fiber membranes for effective removal of ciprofloxacin, Environ. Sci. Technol., 45 (2011) 4003–4009.

[20] Y. Chiang, Y. Hsub, R. Ruaan, C. Chuang, K. Tung, Nanofiltration membranes synthesized from hyperbranched polyethyleneimine, J. Membr. Sci., 326 (2009) 19–26.

[21] D.A. Tomalia, Starburstr dendrimers – nanoscopic supermolecules according to dendritic rules and principles, Macromol. Symp., 101 (1996) 243–255.

[22] X. Zhu, F. Tang, T.S. Suzuki, Y. Sakka, Role of the initial degree of ionization of polyethylenimine in the dispersion of silicon carbide nanoparticles, J. Am. Ceram. Soc., 86 (2003) 189–191.

[23] W. Lixiong, W. Xing, Z. Tianyuan, C. Jianfeng, Effects of polyethylenimine on the dispersibility of hollow silica nanoparticles, J. Chem. Eng. Chin. Univ., 20 (2006) 752–758.

[24] M. Amini, A. Rahimpour, M. Jahanshahi, Forward osmosis application of modified TiO_2-polyamide thin film nanocomposite membranes, Desal. Wat. Treat., 57 (2016) 14013–14023.

[25] N. Ma, J. Wei, R. Liao, C.Y. Tang, Zeolite-polyamide thin film nanocomposite membranes: towards enhanced performance for forward osmosis, J. Membr. Sci., 405–406 (2012) 149–157.

[26] X. Song, L. Wang, C.Y. Tang, Z. Wang, C. Gao, Fabrication of carbon nanotubes incorporated double-skinned thin film nanocomposite membranes for enhanced separation performance and antifouling capability in forward osmosis process, Desalination, 369 (2015) 1–9.

[27] F. Perreault, H. Jaramillo, M. Xie, M. Ude, L.D. Nghiem, M. Elimelech, Biofouling mitigation in forward osmosis using graphene oxide functionalized thin-film composite membranes, Environ. Sci. Technol., 50 (2016) 5840–5848.

[28] H.T. Nguyen, N.C. Nguyen, S.-S. Chen, C.-W. Li, H.-T. Hsu, S.-Y. Wu, Innovation in draw solute for practical zero salt reverse in forward osmosis desalination, Ind. Eng. Chem. Res., 54 (2015) 6067–6074.
[29] A.K. Ghosh, B.-H. Jeong, X. Huang, E.M.V. Hoek, Impacts of reaction and curing conditions on polyamide composite reverse osmosis membrane properties, J. Membr. Sci., 311 (2008) 34–45.
[30] D. Emadzadeh, W.J. Lau, T. Matsuura, N. Hilal, A.F. Ismail, The potential of thin film nanocomposite membrane in reducing organic fouling in forward osmosis process, Desalination, 348 (2014) 82–88.
[31] V. Parida, H.Y. Ng, Forward osmosis organic fouling: effects of organic loading, calcium and membrane orientation, Desalination, 312 (2013) 88–98.
[32] A. Achilli, T.Y. Cath, E.A. Marchand, A.E. Childress, The forward osmosis membrane bioreactor: a low fouling alternative to MBR processes, Desalination, 239 (2009) 10–21.
[33] Y. Gu, Y.N. Wang, J. Wei, C.Y. Tang, Organic fouling of thin-film composite polyamide and cellulose triacetate forward osmosis membranes by oppositely charged macromolecules, Water Res., 47 (2013) 1867–1874.
[34] B. Mi, M. Elimelech, Chemical and physical aspects of organic fouling of forward osmosis membranes, J. Membr. Sci., 320 (2008) 292–302.
[35] Y. Liu, B. Mi, Effects of organic macromolecular conditioning on gypsum scaling of forward osmosis membranes, J. Membr. Sci., 450 (2014) 153–161.